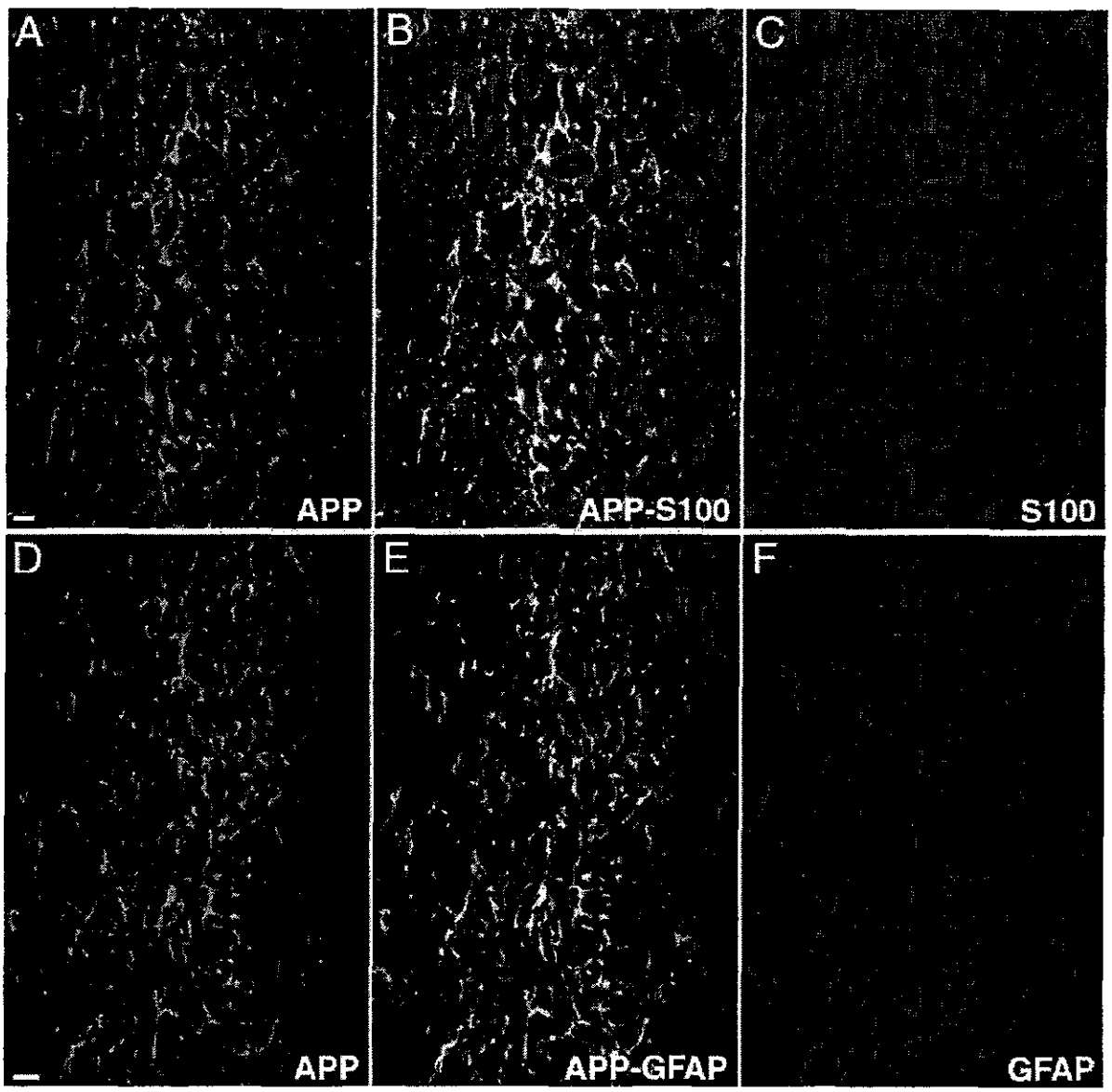

Fig. 5 (A–F) Pseudocolour images of double-immunofluorescent labelling for *APP* and one for the *glial markers S-100* (A–C) or GFAP (D–F), in coronal sections of the SEZre. (A–C) Images of FITC-labelled APP-like-ir elements (A) and Texas red-labelled S-100-ir elements (C), and their superimposed image (B), of a single optical section. In the core of SEZre, APP-like immunoreactivity was co-localized with the processes of S-100-ir astrocytes forming 'glial tubes' (yellow in B). Note that S-100 immunoreactivity occurs throughout the glial cells, including the cytoplasm and the nucleus. (D–F) Images of FITC-labelled APP-like-ir elements (D) and Texas-red-labelled GFAP-ir elements (F), and their superimposed image (E), which were reconstructed from a series of ten optical sections. In the core of the SEZre, all APP-like-ir processes express GFAP (yellow and yellowish green in E). Note that GFAP immunoreactivity is restricted to the cytoplasmic processes, and is distinct from S-100 immunoreactivity (C). Scale bars = 10 μm.

RMS (reviewed by Alvarez-Buylla & Garcia-Verdugo, 2002). In the present study, double immunolabelling with PSA-NCAM showed that PSA-NCAM-positive neuroblasts in the SVZ make contact with the process of APP-like-ir cells. This suggests that the rostral migration of neuroblasts within the SVZ is possibly performed along the shafts of their long process.

In the RMS, the APP-like-ir structure forms an elaborate meshwork. Double immunofluorescent labelling with S-100 or GFAP showed that the APP-like-ir

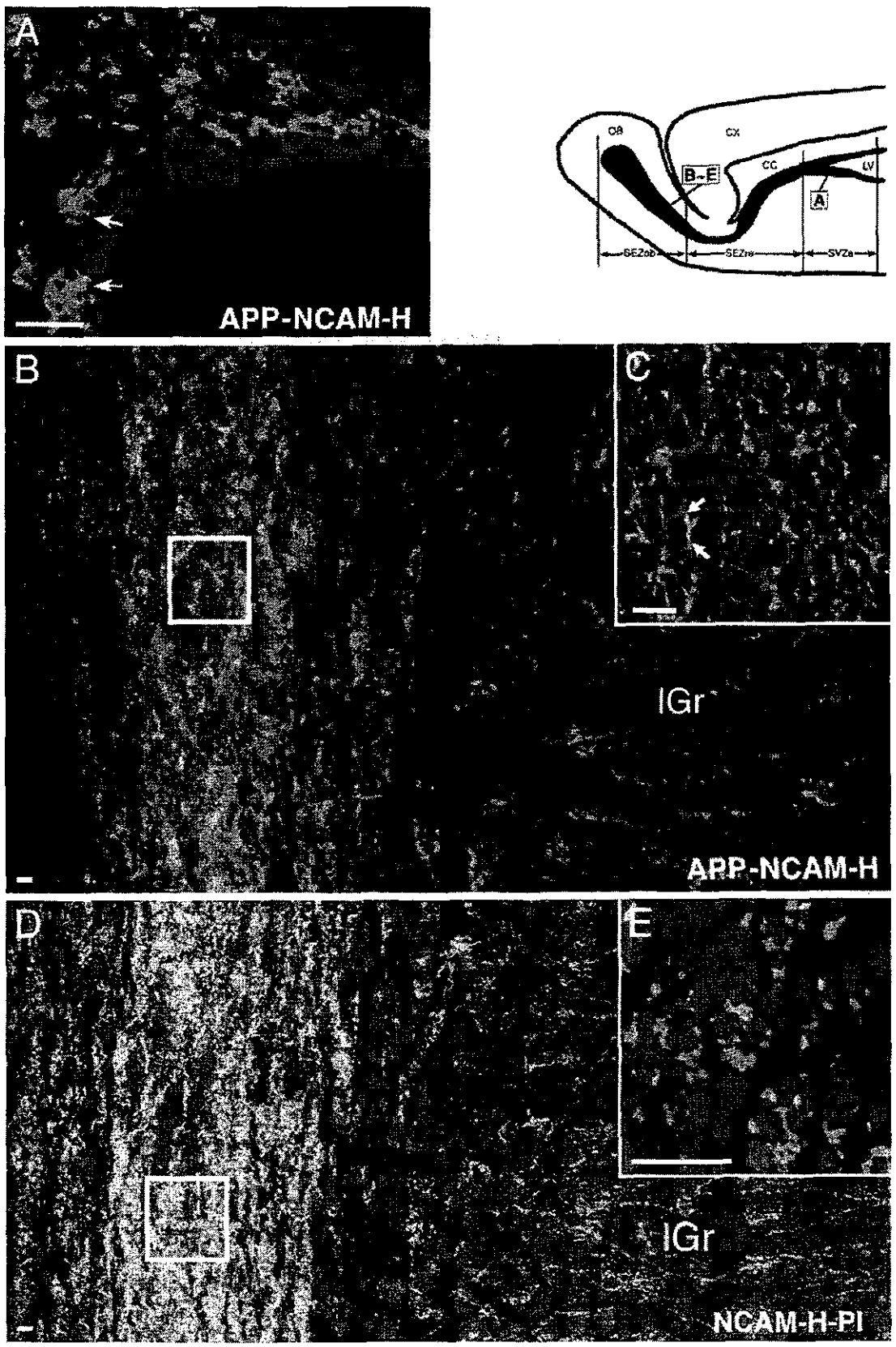

meshwork consisted of astrocyte processes that form tangentially orientated 'glial tubes' (Peretto et al. 1997). These astrocytes also had immature properties, such as the presence of vimentin and glycogen granules in their processes (Peretto et al. 1997). Peretto et al. (1997) suggested that glial tubes could play a role in a unique type of glial guidance that is specifically linked to the peculiar mode of tangential migration of newly generated cells. Here we confirm that PSA-NCAM-ir neuroblasts are densely packed with the APP-like-ir glial tube throughout the RMS. Thus, APP-like-ir astrocytes in the RMS may act as a guide for the migration of neural precursors. However, Wichterle et al. (1997) challenged this assumption from the results of an *in vivo* model of 'chain migration' (Lois et al. 1996). That is, neural precursors could assemble into a chain and migrate along each other without the assistance of ensheathing astrocytes. They assumed that glial cells only play a role in isolating the migrating precursors from the surrounding parenchyma or provide factors for the survival and direction of young migrating neurons. Hence it cannot be determined whether the expression of APP (and possibly APLP2) in the glial tube implicates this protein in the guidance of the neural precursors or in other functions.

The identification of stem cells is crucial for attempts to prepare these cells for therapeutic applications in the future (reviewed by Alvarez-Buylla & Garcia-Verdugo, 2002). Doetsch et al. (1999) revealed that astrocytes in the SVZ are unexpected precursors of new neurons *in vivo* and give rise to cells that grow into multipotent neurospheres *in vitro*. Furthermore, astrocytes in the hippocampus (Seri et al. 2001) and other cell types with astrocytic properties, such as radial glia in the developing neocortex (Malatesta et al. 2000; Miyata et al. 2001; Noctor et al. 2001; Gotz et al. 2002), and Müller cells in the developing retina (reviewed by Fischer & Reh, 2003), have been shown to possess neurogenic potential. Alvarez-Buylla & Garcia-Verdugo (2002) concluded that neural stem cells are contained within the astroglial lineage. By contrast, Johansson et al. (1999) demonstrated that ependymal cells give rise to a rapidly proliferating cell type that generates neurons that migrate to the OB. Thus, the identification of stem cells in the SVZ continues to be disputed, but it is noteworthy that any one of the cell types, i.e. ependymal cells, subependymal astrocytes in the SVZ and astrocytes in the RMS, were positive for mAb 22C11.

The present study has shown that APP-like immunoreactivity was localized to specific subpopulations of cells in the SVZ–OB system of the adult rat forebrain. This region of the adult forebrain could be useful as an *in vivo* model to investigate the role of APP in neurogenesis.

Acknowledgements

We thank Mr Takaaki Kanemaru (Morphology Core, Faculty of Medicine, Kyushu University) for help in preparing the photomicrographs. This work was supported by a Grant-in-Aid for Scientific Research from the Japanese Ministry of Education, Science and Culture (12000210, 12670018).

References

Alvarez-Buylla A, Garcia-Verdugo JM (2002) Neurogenesis in adult subventricular zone. *J. Neurosci.* **22**, 629–634.

Banati RB, Gehrmann J, Kreutzberg GW (1994) Glial beta-amyloid precursor protein: expression in the dentate gyrus after entorhinal cortex lesion. *Neuroreport* **5**, 1359–1361.

Beeson JG, Shelton ER, Chan HW, Gage FH (1994) Differential distribution of amyloid protein precursor immunoreactivity in the rat brain studied by using five different antibodies. *J. Comp. Neurol.* **342**, 78–96.

Bonfanti L, Theodosis DT (1994) Expression of polysialylated

Fig. 6 Relationship between APP-like-ir elements and PSA-NCAM-ir elements in the SVZa (A) and the SEZob (B, C), and the distribution of PSA-NCAM-ir neuronal precursor cells in the SEZob (D, E). (A–C) Pseudocolour images of double-immunofluorescent labelling for APP (red) and PSA-NCAM (green). (A) A single optical section shows that clusters of PSA-NCAM-ir neuroblasts, located under a layer of APP-like-ir ependymal and subependymal cells, are loosely enclosed by APP-like-ir networks. Arrows indicate contact between these elements. (B) A three-dimensional image, reconstructed from a series of ten sections, shows that clusters of PSA-NCAM-ir neuroblasts are more numerous compared with A, and are tightly enclosed by APP-like-ir networks of 'glial tubes' in the core. PSA-NCAM-ir elements spread beyond the limits of the core toward the internal granular layer (IGr), suggesting 'radial migration' of neuroblasts. (C) Higher magnification of a single optical section of the region corresponding to the white box in B shows that two elements are often in close contact. Yellowish green indicates the close apposition (arrows). (D, E) Pseudocolour images of double-immunofluorescent labelling for PSA-NCAM (green and yellow) and nuclear staining with PI (red). (D) Three-dimensional images, reconstructed from a series of ten sections, show that the distribution of PSA-NCAM-ir neuroblasts in the SEZob is clearly indicated by PI nuclear staining. (E) Higher magnification of a single optical section in the white box in D shows that PSA-NCAM immunoreactivity is detected in cells with PI-stained nuclei. Scale bars = 10 μm.

neural cell adhesion molecule by proliferating cells in the subependymal layer of the adult rat, in its rostral extension and in the olfactory bulb. *Neuroscience* **62**, 291–305.

Chauvet N, Apert C, Dumoulin A, Epelbaum J, Alonso G (1997) Mab22C11 antibody to amyloid precursor protein recognizes a protein associated with specific astroglial cells of the rat central nervous system characterized by their capacity to support axonal outgrowth. *J. Comp. Neurol.* **377**, 550–564.

Dahl D, Rueger DC, Bignami A, Weber K, Osborn M (1981) Vimentin, the 57 000 molecular weight protein of fibroblast filaments, is the major cytoskeletal component in immature glia. *Eur. J. Cell Biol.* **24**, 191–196.

Doetsch F, Alvarez-Buylla A (1996) Network of tangential pathways for neuronal migration in adult mammalian brain. *Proc. Natl Acad. Sci. USA* **93**, 14895–14900.

Doetsch F, Garcia-Verdugo JM, Alvarez-Buylla A (1997) Cellular composition and three-dimensional organization of the subventricular germinal zone in the adult mammalian brain. *J. Neurosci.* **17**, 5046–5061.

Doetsch F, Caille I, Lim DA, Garcia-Verdugo JM, Alvarez-Buylla A (1999) Subventricular zone astrocytes are neural stem cells in the adult mammalian brain. *Cell* **97**, 703–716.

Esch FS, Keim PS, Beattie EC, et al. (1990) Cleavage of amyloid beta peptide during constitutive processing of its precursor. *Science* **248**, 1122–1124.

Fischer AJ, Reh T (2003) A. Potential of Müller glia to become neurogenic retinal progenitor cells. *Glia* **43**, 70–76.

Gates MA, Thomas LB, Howard EM, et al. (1995) Cell and molecular analysis of the developing and adult mouse subventricular zone of the cerebral hemispheres. *J. Comp. Neurol.* **361**, 249–266.

Goldgaber D, Lerman MI, McBride OW, Saffiotti U, Gajdusek DC (1987) Characterization and chromosomal localization of a cDNA encoding brain amyloid of Alzheimer's disease. *Science* **235**, 877–880.

Gotz M, Hartfuss E, Malatesta P (2002) Radial glial cells as neuronal precursors: a new perspective on the correlation of morphology and lineage restriction in the developing cerebral cortex of mice. *Brain Res. Bull.* **57**, 777–788.

He JW, Hirata K, Kuraoka A, Kawabuchi M (2000) An improved method for avulsion of lumbar nerve roots as an experimental model of nitric oxide-mediated neuronal degeneration. *Brain Res. Protcol.* **5**, 223–230.

Hilbich C, Monning U, Grund C, Masters CL, Beyreuther K (1993) Amyloid-like properties of peptides flanking the epitope of amyloid precursor protein-specific monoclonal antibody 22C11. *J. Biol. Chem.* **268**, 26571–26577.

Johansson CB, Momma S, Clarke DL, Risling M, Lendahl U, Frisen J (1999) Identification of a neural stem cell in the adult mammalian central nervous system. *Cell* **96**, 25–34.

Kang J, Lemaire HG, Unterbeck A, et al. (1987) The precursor of Alzheimer's disease amyloid A4 protein resembles a cell-surface receptor. *Nature* **325**, 733–736.

Lois C, Alvarez-Buylla A (1994) A. Long-distance neuronal migration in the adult mammalian brain. *Science* **264**, 1145–1148.

Lois C, Garcia-Verdugo JM, Alvarez-Buylla A (1996) Chain migration of neuronal precursors. *Science* **271**, 978–981.

Malatesta P, Hartfuss E, Gotz M (2000) Isolation of radial glial cells by fluorescent-activated cell sorting reveals a neuronal lineage. *Development* **127**, 5253–5263;.

Miyata T, Kawaguchi A, Okano H, Ogawa M (2001) Asymmetric inheritance of radial glial fibers by cortical neurons. *Neuron* **31**, 727–741.

Morimoto T, Ohsawa I, Takamura C, Ishiguro M, Nakamura Y, Kohsaka S (1998a) Novel domain-specific actions of amyloid precursor protein on developing synapses. *J. Neurosci.* **18**, 9386–9393.

Morimoto T, Ohsawa I, Takamura C, Ishiguro M, Kohsaka S (1998b) Involvement of amyloid precursor protein in functional synapse formation in cultured hippocampal neurons. *J. Neurosci. Res.* **51**, 185–195.

Mucke L, Masliah E, Johnson WB, et al. (1994) Synaptotrophic effects of human amyloid beta protein precursors in the cortex of transgenic mice. *Brain Res.* **666**, 151–167.

Noctor SC, Flint AC, Weissman TA, Dammerman RS, Kriegstein AR (2001) Neurons derived from radial glial cells establish radial units in neocortex. *Nature* **409**, 714–720.

Ohsawa I, Takamura C, Kohsaka S (1997) The amino-terminal region of amyloid precursor protein is responsible for neurite outgrowth in rat neocortical explant culture. *Biochem. Biophys. Res. Commun.* **236**, 59–65.

Ohsawa I, Takamura C, Morimoto T, Ishiguro M, Kohsaka S (1999) Amino-terminal region of secreted form of amyloid precursor protein stimulates proliferation of neural stem cells. *Eur. J. Neurosci.* **11**, 1907–1913.

Ohta M, Kitamoto T, Iwaki T, Ohgami T, Fukui M, Tateishi J (1993) Immunohistochemical distribution of amyloid precursor protein during normal rat development. *Brain Res. Dev. Brain Res.* **75**, 151–161.

Ouimet CC, Baerwald KD, Gandy SE, Greengard P (1994) Immunocytochemical localization of amyloid precursor protein in rat brain. *J. Comp. Neurol.* **348**, 244–260.

Palacios G, Palacios JM, Mengod G, Frey P (1992) Beta-amyloid precursor protein localization in the Golgi apparatus in neurons and oligodendrocytes. An immunocytochemical structural and ultrastructural study in normal and axotomized neurons. *Brain Res. Mol. Brain Res.* **15**, 195–206.

Palmer TD, Takahashi J, Gage FH (1997) The adult rat hippocampus contains primordial neural stem cells. *Mol. Cell. Neurosci.* **8**, 389–404.

Peretto P, Merighi A, Fasolo A, Bonfanti L (1997) Glial tubes in the rostral migratory stream of the adult rat. *Brain Res. Bull.* **42**, 9–21.

Peretto P, Merighi A, Fasolo A, Bonfanti L (1999) The subependymal layer in rodents: a site of structural plasticity and cell migration in the adult mammalian brain. *Brain Res. Bull.* **49**, 221–243.

Salbaum JM, Ruddle FH (1994) Embryonic expression pattern of amyloid protein precursor suggests a role in differentiation of specific subsets of neurons. *J. Exp. Zool.* **269**, 116–127.

Sandbrink R, Masters CL, Beyreuther K (1994) Complete nucleotide and deduced amino acid sequence of rat amyloid protein precursor-like protein 2 (APLP2/APPH): two amino acids length difference to human and murine homologues. *Biochem. Biophys. Acta* **1219**, 167–170.

Selkoe DJ (1994) Cell biology of the amyloid beta-protein

precursor and the mechanism of Alzheimer's disease. *Ann. Rev. Cell Biol.* **10**, 373–403.

Seri B, Garcia-Verdugo JM, McEwen BS, Alvarez-Buylla A (2001) Astrocytes give rise to new neurons in the adult mammalian hippocampus. *J. Neurosci.* **21**, 7153–7160.

Sisodia SS, Koo EH, Beyreuther K, Unterbeck A, Price DL (1990) Evidence that beta-amyloid protein in Alzheimer's disease is not derived by normal processing. *Science* **248**, 492–495.

Slunt HH, Thinakaran G, Von Koch C, Lo AC, Tanzi RE, Sisodia SS (1994) Expression of a ubiquitous, cross-reactive homologue of the mouse beta-amyloid precursor protein (APP). *J. Biol. Chem.* **269**, 2637–2744.

Tanzi RE, Gusella JF, Watkins PC, et al. (1987) Amyloid beta protein gene: cDNA, mRNA distribution, and genetic linkage near the Alzheimer locus. *Science* **235**, 880–884.

Trapp BD, Hauer PE (1994) Amyloid precursor protein is enriched in radial glia: implications for neuronal development. *J. Neurosci. Res.* **37**, 538–550.

Wichterle H, Garcia-Verdugo JM, Alvarez-Buylla A (1997) Direct evidence for homotypic, glia-independent neuronal migration. *Neuron* **18**, 779–791.

Zheng H, Jiang M, Trumbauer ME, et al. (1995) Beta-Amyloid precursor protein-deficient mice show reactive gliosis and decreased locomotor activity. *Cell* **81**, 525–531.

GLIA 47:325–334 (2004)

N-myc Downstream-Regulated Gene 1 Expression in Injured Sciatic Nerves

KAZUHO HIRATA,[1]* KATSUAKI MASUDA,[2] WATARU MORIKAWA,[2] JIAN-WEN HE,[1] AKIO KURAOKA,[1] MICHIHIKO KUWANO,[2] AND MASARU KAWABUCHI[1]
[1]*Department of Anatomy and Cell Biology, Graduate School of Medical Sciences, Kyushu University, Fukuoka, Japan*
[2]*Department of Medical Biochemistry, Graduate School of Medical Sciences, Kyushu University, Fukuoka, Japan*

KEY WORDS NDRG1; nerve regeneration; Schwann cells; immunohistochemistry

ABSTRACT N-myc downstream-regulated gene 1 (NDRG1)/RTP/Drg1/Cap43/rit42/TDD5/Ndr1 is expressed ubiquitously and has been proposed to play a role in growth arrest and cell differentiation. A recent study showed that mutation of this gene is responsible for hereditary motor and sensory neuropathy-Lom. However, the role of this gene in the peripheral nervous system is not fully understood. In our study, rabbit polyclonal antibodies were raised against this gene product and were used to examine changes in its expression over the time course of Wallerian degeneration and ensuing regeneration after crush injury of mouse sciatic nerves. Fluorescent immunohistochemistry showed that NDRG1 was expressed over the intact nerve fibers. Double labeling with a Schwann cell (SC) marker, S-100 protein (S-100), revealed that NDRG1 was localized in the cytoplasm of S-100-positive Schwann cells (SCs). NDRG1 expression was maintained in the early stage of myelin degradation but was then markedly depleted at the end stage of myelin degradation when frequent occurrence of BrdU-labeled SCs was observed (at 7–9 days). The depletion of NDRG1 at this time point was also confirmed by Western blotting analysis. NDRG1 expression finally recovered at the stage of remyelination, with immunoreactivity stronger than that in intact nerves. These findings suggest that NDRG1 may play an important role in the terminal differentiation of SCs during nerve regeneration.

INTRODUCTION

N-myc downstream-regulated gene 1 was originally designated reducing agent and tunicamycin-responsive protein (RTP) (Kokame et al., 1996), homologues of which were then isolated repeatedly: human differentiation-related gene 1 (Drg1) (van Belzen et al., 1997), human protein induced by free intracellular Ca^{2+} (Cap43) (Zhou et al., 1998), the mouse homologue designated TDD5 (Lin and Chang, 1997), reduced in tumor, p43 (rit42) (Kurdistani et al., 1998), and N-myc-downstream, repressed gene 1 (Ndr1) (Shimono et al., 1999). Currently the official name of this gene is NDRG1, determined by the HUGO Gene Nomenclature Committee (Qu et al., 2002). We have adopted the nomenclature NDRG1 in this report. A recent study showed that NDRG1 is a member of the NDRG gene family that contains an α/-β-hydrolase fold (Qu et al., 2002) without the residues required for catalysis (Shaw et al., 2002). It encodes a highly conserved protein with a high degree of homology to the proteins in other species, such as zebrafish (Gen Bank Accession Nos. AW281236 and AI657643), fruit flies (AF145604 and AE003454), nematodes (Z68135 and AL132847), sunflowers (Y09057 and AF189147) (Krauter-Canham et al., 1997), and *Arabidopsis* (AC005917 and AL163814). The evolutional conservation of this gene implies that it plays an important biological role. This gene has been reported to be involved in cell growth and differ-

*Correspondence to: Kazuho Hirata, Department of Anatomy and Cell Biology, Graduate School of Medical Sciences, Kyushu University, Higashi-ku, Maidashi 3-1-1, Fukuoka, 812-8582 Japan. E-mail: hirata@anat1.med.kyushu-u.ac.jp

Received 20 September 2003; Accepted 29 January 2004
DOI 10.1002/glia.20037
Published online 30 April 2004 in Wiley *Inter*Science (www.interscience.wiley.com).

entiation (van Belzen et al., 1997; Piquemal et al., 1999; Shimono et al., 1999; Gomez-Casero et al., 2001), stress responses (Kokame et al., 1996; Xu et al., 1999; Agarwala et al., 2000; Salnikow et al., 2000; Segawa et al., 2002), and hormone responses (Lin and Chang, 1997; Ulrix et al., 1999; Segawa et al., 2002). Of particular interest is the observation that NDRG1 may have a complex but important function in carcinogenesis (Guan et al., 2000; Salnikow et al., 2000; Gomez-Casero et al., 2001; Nishie et al., 2001; Segawa et al., 2002; Bandyopadhyay et al., 2003) and atherogenesis (Kokame et al., 1996; Sato et al., 1998). Furthermore, attention has been drawn to the fact that this gene was identified as a gene responsible for hereditary motor and sensory neuropathy-Lom (HMSNL) (Kalaydjieva et al., 2000), which is an autosomal recessive form of Charcot-Marie-Tooth disease (CMT) and an early-onset peripheral neuropathy that progresses to severe disability in adulthood. However, the precise role of NDRG1 in the peripheral nervous system (PNS) remains to be elucidated.

It is well known that after axotomy the PNS has the capacity to be repaired by the established sequential process of Wallerian degeneration and ensuing regeneration (for review, see Hirata and Kawabuchi, 2002). Our previous studies (Hirata et al., 1999; Hirata et al., 2000, 2003) obtained stable and consistent results for the time course of the cellular and molecular events seen in the distal stump of the sciatic nerves following crush injury. It is expected that this crush injury model will provide useful clues for exploring the role of NDRG1 in the PNS. In the present study, polyclonal antibody (pAb) was raised against NDRG1 and was used for immunofluorescent labeling of mouse sciatic nerves after crush injury. The results showed that the expression of NDRG1, which was localized in the cytoplasm of Schwann cells (SCs) in intact nerves, dramatically changed during the process of regeneration. The role of the NDRG1 in the PNS is discussed.

MATERIALS AND METHODS

Production of Polyclonal Anti-NDRG1 Antisera

Synthetic peptides corresponding to internal sequences of human NDRG1 were prepared and used as immunogens. These included the TSEGTRSRSC sequence that corresponds to the tandem repetitive region unique to NDRG1 (Kokame et al., 1996; Okuda and Kondoh, 1999; Shimono et al., 1999). The peptides were coupled with keyhole limpet hemocyanin (KLH) and were used to immunize rabbits.

Immunoblotting Analysis

The sciatic nerves of the intact side and the proximal and distal stumps of the operated side at 9 days after the crush injury were homogenized in 500 ml of 1 mM $NaHCO_3$ buffer (pH 7.2) and centrifuged at 9,000 *g* for 15 min at 4°C. The supernatants were subjected to SDS-PAGE and immunoblotting analysis as described previously (Yamanaka et al., 1997), using a pAb to NDRG1 and peroxidase-conjugated goat anti-rabbit IgG (Jackson, West Grove, PA) diluted at 1:1,000 and 1:10,000, respectively.

TABLE 1. Other Primary Antibodies Used in Immunohistochemical Procedures

Antibody (clone)	Structure/ cell recognized	Source	Dilution	Species
MBP	Myelin	Chemicon	1:100	Rat
NF (NE14)	Axons	Boehringer	1:20	Mouse
S-100	Schwann cells	Bio Makor	1:1000	Mouse
BrdU (biotinylated)	Proliferating cells	Oncogene	Ready-to-use	Mouse
S-100	Schwann cells	Nichirei	1:10	Rabbit

Surgical Procedures

Adult male mice (C57BL6) weighing 20–25 g were used for all experiments. The left sciatic nerve was crushed for 30 s with jeweler's forceps at the mid-thigh level under pentobarbital anesthesia. After the surgery, kanamycin sulfate was sprayed over the entire surgical area and the wound was sutured. The intact contralateral side served as a control. Three mice were sacrificed on each of days 1, 2, 3, 7, 9, 14, and 21 after the operation.

The animals were anesthetized with ether, followed by intracardiac perfusions with 0.01 M phosphate-buffered saline (PBS) and then 4% paraformaldehyde in 0.1 M phosphate buffer (PB). The sciatic nerves were removed at a length of about 6 mm, and consisted of the proximal part (2-mm length), the crush injury site (1-mm length) and the distal part (3-mm length). The segments were postfixed with the same fixative for 3 h and immersed in 15% sucrose in 0.1M PB. They were then embedded in Embedding Matrix and immediately frozen with dry ice and isopentane. Longitudinal and transverse serial sections (10-μm thickness) were cut by using a cryostat microtome.

Immunohistochemistry

The immunohistochemical procedure used in the present study has been described elsewhere (Hirata et al., 2003). Briefly, cryostat sections were fixed again with 100% methanol for 10 min at −20°C and then washed with PBS. Nonspecific binding sites were blocked by preincubation with 1% bovine serum albumin (BSA) or 10% Block Ace (Yukijirushi, Sapporo, Japan) in PBS for 1 h at room temperature (RT). For NDRG1 immunohistochemistry, sections were first incubated with a pAb to NDRG1 diluted 1:100 in PBS overnight at RT and then with fluorescein isothiocya-

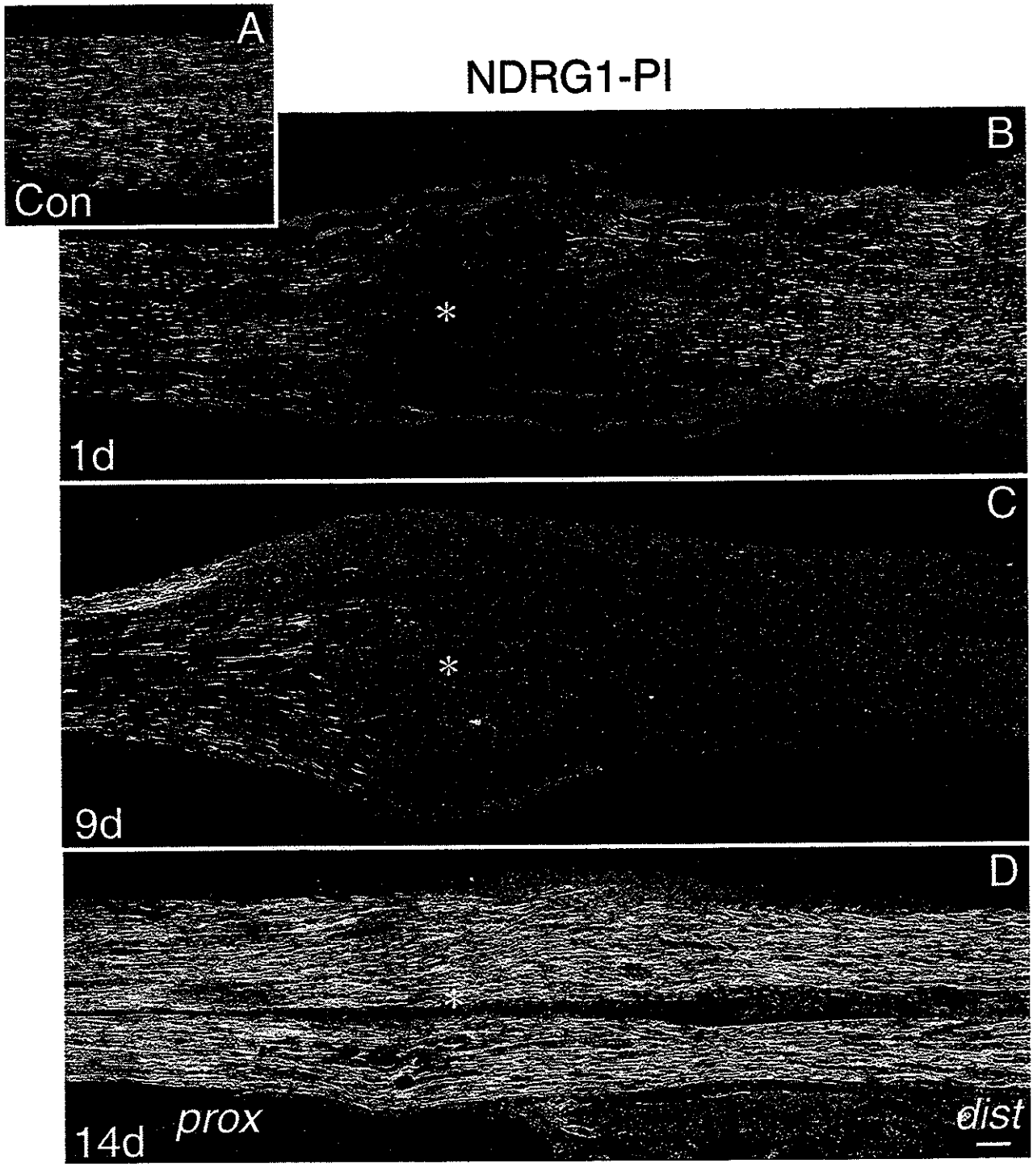

Fig. 1. Expression of NDRG1 (green) in longitudinal sections of intact sciatic nerve used as a control (**A**) and sciatic nerves at 1 day (**B**), 9 days (**C**), and 14 days (**D**) after crush injury. Moderate NDRG1-immunoreactive (-ir) structures seen in the intact nerve (A) remain in the distal stump at 1 day (B), but are hardly detected there at 9 days (C). The NDRG1-ir structures reappear with stronger immunoreactivity than that in the intact nerves at 14 days (D). Asterisks show the crush injury site. The distal and proximal stumps are indicated by dist and prox, respectively. Red indicates nuclei stained by PI. Scale bar = 50 μm

nate (FITC)-conjugated horse anti-rabbit IgG (Vector, Burlingame, CA) for 4 h at room temperature (RT). Control sections were processed identically and in parallel, except that they were incubated with PBS instead of the pAb to NDRG1. No stained cells were seen in these controls. To identify the nuclei of the cells, the

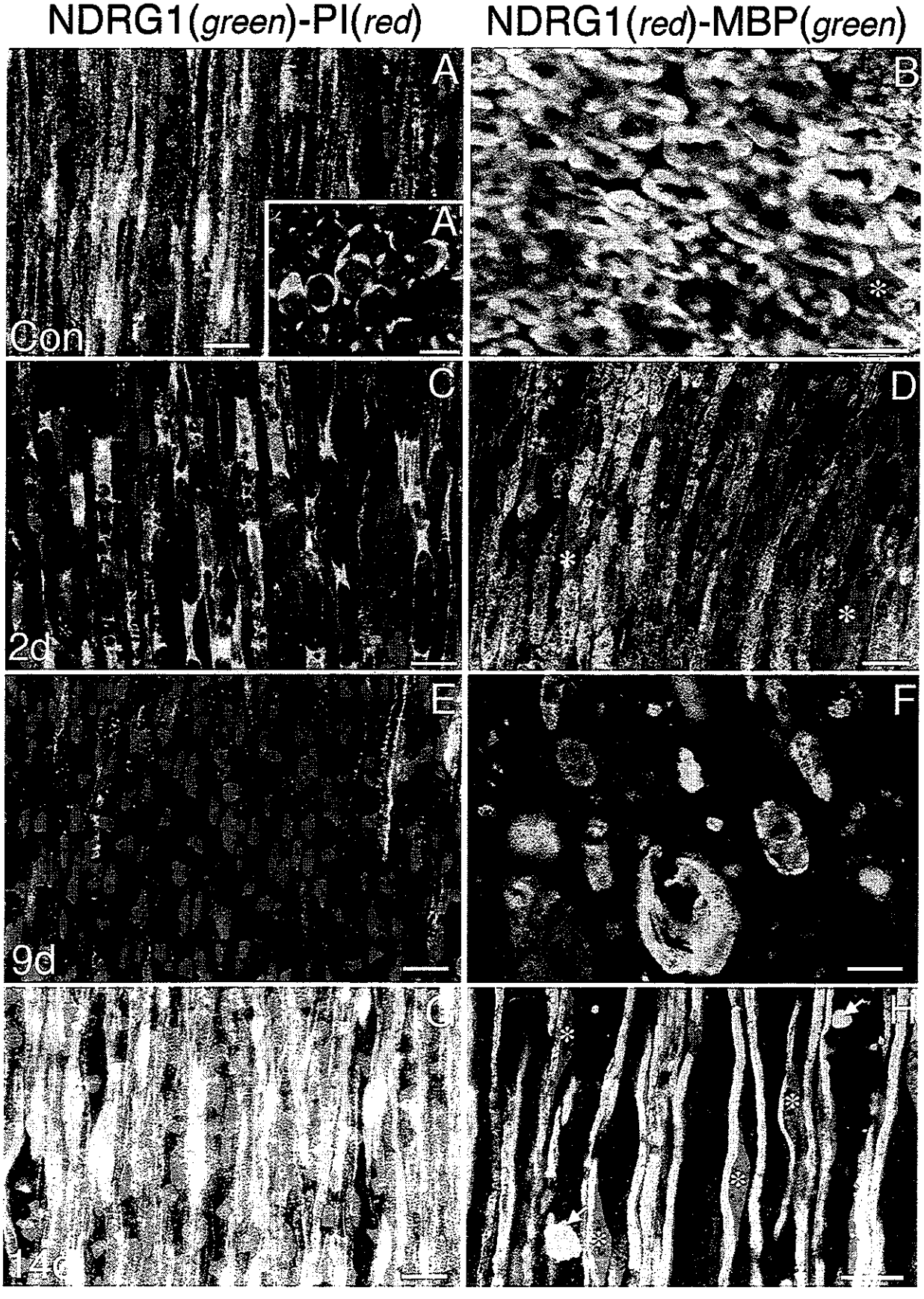
NDRG1(green)-PI(red)
NDRG1(red)-MBP(green)
A
A'
B
Con
C
D
2d
E
F
9d
G
H
14d

Figure 2.

sections were counterstained with propidium iodide (PI) by using a Vectashield mounting medium containing PI (Vector).

To understand the time course of Wallerian degeneration and ensuing regeneration, double immunofluorescent labeling of NDRG1 with a myelin marker (Table 1) was performed. A mixture of a rabbit pAb to NDRG1 and a rat monoclonal antibody (mAb) to myelin basic protein (MBP) was used as the primary antibody. Then, a mixture of Texas red-conjugated donkey anti-rabbit IgG (Jackson) and FITC-conjugated donkey anti-rat IgG (Jackson) was used as the secondary antibody.

Furthermore, double immunofluorescent labeling of NDRG1 with axonal or SC markers (Table 1) was performed. A mixture of a rabbit pAb to NDRG1 and either a mouse mAb to 200-kDa neurofilament protein (NF) or to a mouse mAb to S-100 protein (S-100) was used as the primary antibody. Then, a mixture of FITC-conjugated horse anti-mouse IgG (Vector) and Texas red-conjugated donkey anti-rabbit IgG (Jackson) was used as the secondary antibody. No difference in morphology was noted in any of the immunolabeled structures between the single and double labeling.

To identify mitotic activity of SCs, double immunofluorescent labeling of bromodeoxyuridine (BrdU) and S-100 (Table 1) was performed. Mice were injected intraperitoneally with BrdU (Zymed, CA) (1 ml/100 g) 2 h or 2.5 h prior to being sacrificed. The nerve sections were incubated with a pAb to S-100 as a primary antibody and visualized by Texas red-conjugated donkey anti-rabbit IgG. For subsequent BrdU labeling, part of a BrdU staining kit (Oncogene Research, MA) was used; after treatment with HCl, the biotinylated mouse mAb to BrdU was used as primary antibody. The BrdU binding sites were visualized with streptavidin-FITC (Vector). Double immunofluorescent labeling of NDRG1 and BrdU was attempted, but was unsuccessful since the anti-NDRG1 staining was not compatible with the HCl treatment required for BrdU detection.

Confocal Laser Scanning Microscopy

The sections double-labeled with FITC and PI or FITC and Texas red were scanned with a confocal laser scanning imaging (CLSM) system (LSM-GB200, Olympus, Japan) using excitations at 488 nm (argon laser) for FITC and 568 nm (krypton laser) for PI or Texas red. Single optical sections for each fluorescence were taken separately (channel 1 and channel 2) to avoid any cross-talk and then superimposed. The images were taken using a ×10, ×20, ×40, or ×60 objective lens.

These experiments were reviewed by the Committee on Ethics for Animal Experiments of the Faculty of Medicine, Kyushu University and carried out according to the Guidelines for Animal Experiments of the University, and Law No. 105 and Notification No. 6 of the Japanese government.

RESULTS

In intact sciatic nerves, NDRG1 was expressed over the nerve (Fig. 1A). At 1 day after the crush injury, the expression showed no change except for its disappearance at the injury site (Fig. 1B). At 7–9 days after the crush injury, drastic depletion of the NDRG1 expression was seen at the injury site and the distal stump (Fig. 1C). The expression of NDRG1 then recovered at the injury site and the distal stump at 14 days after the crush injury, showing a slight increase in the immunoreactivity compared to that in the intact nerve (Fig. 1D). Higher magnification of longitudinal (Fig. 2A) and transverse (Fig. 2A′) sections of the intact nerve double-stained with PI nuclear staining showed that NDRG1 immunoreactivity was usually localized in the perinuclear cytoplasm of presumptive SCs of each fiber. Double immunofluorescent labeling with MBP revealed that MBP-immunoreactive (-ir) myelin sheath was usually surrounded by NDRG1-ir cytoplasm (Fig. 2B). At 2 days, cells in the distal stump transformed into cells containing various size of vacuoles, which are known to be characteristic for myelin-phagocytosing cells (Fig. 2C) and double labeling with MBP showed that MBP-ir degraded myelin structures were contained in the vacuoles of NDRG1-ir cells (Fig. 2D). At 7–9 days, NDRG1-ir cells were hardly detected in the injury site (Fig. 2E) and distal stumps (Fig. 2F), where the clearance of myelin debris was considerably progressed (Fig. 2F). At 2 weeks, numerous NDRG1-ir cells with a regular profile similar to that in intact nerves reappeared and the immunoreactivity was stronger than that in the intact nerve (Fig. 2G), and double labeling with MBP revealed that NDRG1-ir cells were in the process of myelinating (Fig. 2H).

Fig. 2. Pseudocolor images of double labeling of NDRG1 (green) with PI (red) (left panel: **A,A′,C,E,G**) and of double immunofluorescent labeling of NDRG1 (red) and MBP (green) (right panel: **B,D,F,H**) of intact nerves (A,A′,B), and of the injury site (E) and the distal stump (C,D,F–H) of crush-injured nerves. All pictures are from longitudinal sections, except for A′,B, which are from transverse sections. Asterisks (B,D,H) indicate sites of nuclei. **A,A′,B:** In intact nerves NDRG1 immunoreactivity is detectable in the perinuclear region of cytoplasm of the presumptive Schwann cells (green in A,A′). **B:** NDRG1-ir cells are myelinating cells, in which MBP-ir myelin sheath (green) are surrounded by a thin layer of NDRG1-ir cytoplasm (red). **C,D:** At 2 days, NDRG1-ir cells (green in C, red in D) have transformed into myelin-phagocytosing cells. D: The vacuoles of the cells seen in C are occupied by MBP-ir degraded myelin structures (green). **E,F:** At 9 days, no clearly stained NDRG1 -ir cells are seen both in the injury site (E) and the distal stump (F). E: Small number of NDRG1 cells seen at the boundary toward the proximal stump (upper). Note that only MBP-ir myelin debris can be seen (green in F). **G,H:** At 14 days, the NDRG1-ir cells reappear showing immunoreactivity stronger (G) than that in the intact nerve (A). H: NDRG1-ir cells are just forming a myelin sheath, judging from the prominent profiles of the perinuclear region (red) and thin MBP-ir myelin sheath (green). Note that strong NDRG1 immunoreactivity is seen not only in the perinuclear region also in the nuclear sites of some cells, suggesting translocation of the protein into nucleus. Arrows indicate the myelin debris. Scale bar = 10 μm.

To identify NDRG1-ir elements, double immunofluorescent labeling with NF, a neuronal marker, or S-100, an SC marker, was carried out. In the cross section of the intact nerve, the NDRG1-ir structure could clearly be distinguished from the NF-ir axons, since the former was localized in the peripheral region of a nerve fiber so that it appeared as a ring-like structure and the latter was in the central part (Fig. 3A). In contrast, the immunoreactive sites of NDRG1 were almost identical with those of S-100 in the intact nerve, suggesting that the NDRG1 was contained only in SCs (Fig. 3B,C). NDRG1 continued to be expressed in S-100-ir SCs, which had the characteristics of myelin-phagocytosing cells at 2 days after the crush injury (Fig.3D,E). At the next stage (7–9 days), the expression of NDRG1 was markedly reduced, whereas the S-100-ir SCs were further transformed to cells with irregular contour (Fig. 3F,G). At the ensuing stage (2 weeks), NDRG1 was reexpressed in S-100-ir SCs, which now showed a regular structure similar to that in the intact nerves.

In the process of nerve regeneration, SCs are known to proliferate following transformation into myelin-phagocytosing cells, and then acquire the immature phenotype to promote axonal regrowth (for review, see Hirata and Kawabuchi, 2002). Double immunofluorescent labeling of BrdU and S-100 was carried out to identify the mitotic activity of SCs. In intact nerves, no cells with BrdU-labeled nuclei were found. At 2 days, only a few S-100-ir SCs with BrdU-labeled nuclei appeared, although presumptive macrophages with BrdU-labeled nuclei were often observed in the perineurium or the epineurium. At 7–9 days (Fig. 4A,C), when the transient depletion of NDRG1 expression occurred, numerous SCs with BrdU-labeled nuclei were detected and distributed throughout the injury site and the distal stump. At 2 weeks, the number of cells with BrdU-labeled nuclei markedly decreased. Thus, the results suggested an inverse relationship between the proliferative activity and NDRG1 expression of SCs. The specificity of BrdU labeling was confirmed in the small intestine (Fig. 4B), where the cells with BrdU-labeled nuclei were specifically distributed in the base of the crypts, known to be the proliferative zone (Potten et al., 1997).

Immunoblotting analysis of sciatic nerves at 9 days after the crush injury revealed that the pAb to NDRG1 labeled a polypeptide band of 43 kDa in the intact nerve (Fig. 5B, lane 1) and the proximal stumps (Fig. 5B, lane 2) but not the distal stumps (Fig. 5B, lane 3) of the crushed nerve. This finding not only confirmed the specificity of the antibody but also indicated preferential depletion of NDRG1 molecules in the injured nerves at this time point. No specific labeling was observed in the control probed with normal rabbit sera.

DISCUSSION

In the present study, immunofluorescent histochemistry and Western blotting analysis using NDRG1 antibodies demonstrated that NDRG1 was expressed in intact mouse sciatic nerve. Double immunofluorescent labeling with an SC marker (S-100) or an axonal marker (NF) showed that NDRG1 was localized in the cytoplasm of SCs, but not in the axons. These findings agree with those of human peripheral nerves analyzed by Northern blotting and RT-PCR (Kalaydjieva et al., 2000) and an immunoenzyme-histochemical technique (Lachat et al., 2002).

Double immunofluorescent labeling of NDRG1 and MBP revealed that NDRG1 was expressed in the cytoplasm of myelinating SCs in intact nerves. Crushed nerves showed little alteration of NDRG1 expression when the myelinating SCs transformed into myelin-phagocytosing cells in the early stage of myelin degradation (Stoll et al., 1989; Hirata et al., 1999). This finding implies that the expression of this protein in SCs is not influenced by either the loss of axonal contact or the transformation of SCs into myelin-phagocytosing cells. Thus, NDRG1 expression does not appear to be regulated during Wallerian degeneration. In contrast, the expression of this protein changed markedly during subsequent process. Both immunohistochemistry and Western blotting analysis demonstrated that NDRG1 expression was dramatically depleted at 7–9 days after the operation, when the myelin removal was considerably progressed. NDRG1 was then reexpressed with more immunoreactivity than that of the intact nerves during remyelination. Thus, our study suggests that NDRG1 may be regulated in the regeneration process of injured nerves.

It is well known that, after taking part in the early stage of myelin removal, SCs proliferate to acquire the immature phenotype and prepare the environments through which regenerating axons grow (for review, see Fawcett and Keynes, 1990; Jessen and Mirsky, 1999; Hirata and Kawabuchi, 2002). In the present study, frequent occurrences of BrdU-labeled SCs were seen at 7–9 days after the crush injury, the timing of which is largely consistent with the occurrence of SC mitosis observed by electron microscopy (O'Daly and Imaeda, 1967). It is noteworthy that the drastic depletion of NDRG1 occurred simultaneously during this period. NDRG1 was reported to be developmentally regulated in embryonic tissues and to be augmented concomitantly with the occurrence of terminal differentiation (Shimono et al., 1999). Direct subtraction of whole mouse embryo cDNAs between the wild type and an N-myc mutant (Shimono et al., 1999) revealed that the NDRG1 gene was repressed by N-myc, a member of the myc family that encodes nuclear phosphoproteins and is believed to play a role in the control of cellular proliferation and differentiation (Melhem et al., 1992). Several lines of in vitro evidence have suggested a role for NDRG1 in cells undergoing terminal differentiation. For example, the NDRG1 gene was upregulated during the differentiation of colon carcinoma cell lines cultured in low glucose medium (van Belzen et al., 1997) and during in vitro forskolin-induced differentiation of a model of the human trophoblast, the chorio-

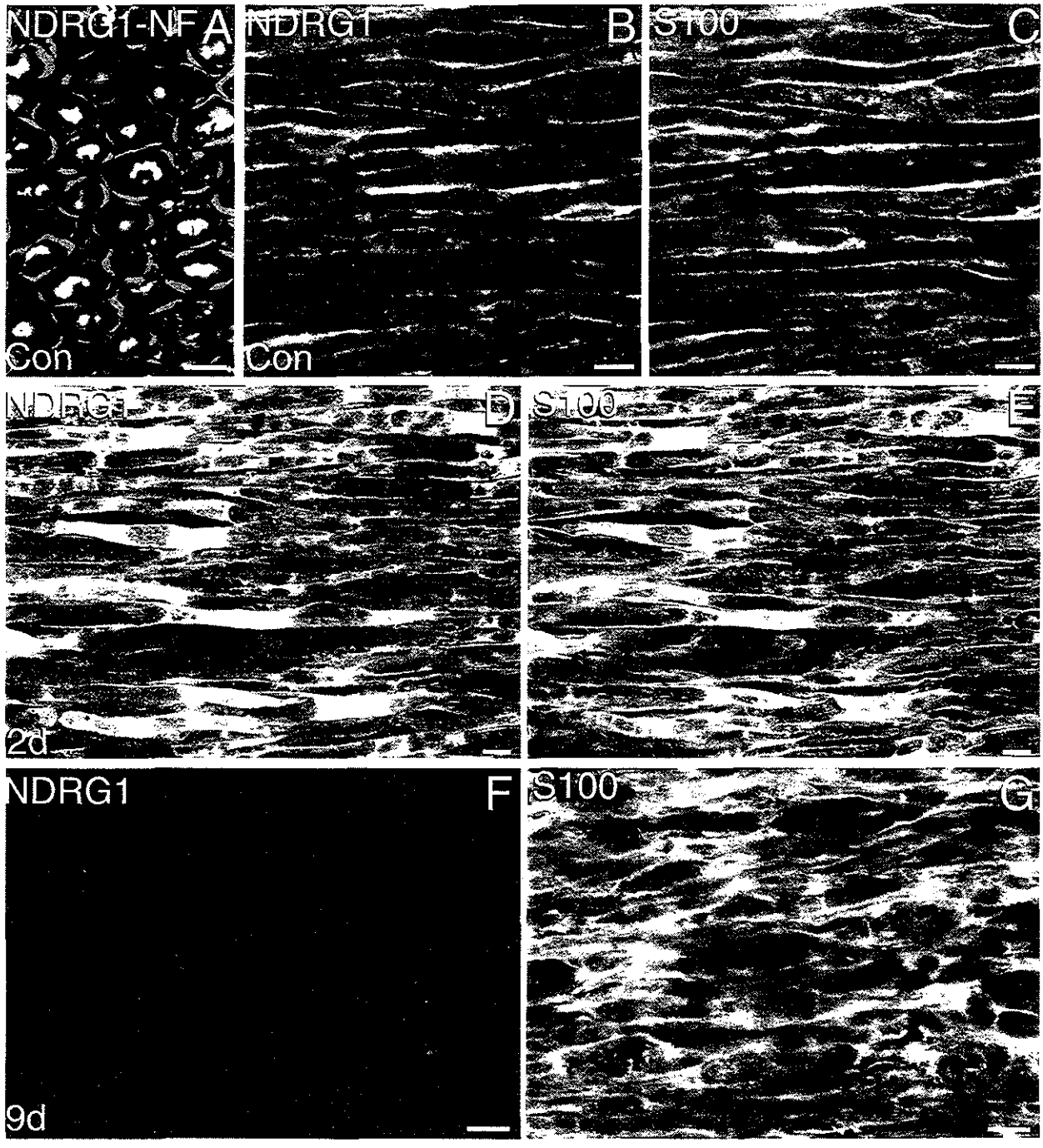

Fig. 3. Gray scale image of double immunofluorescent labeling of NDRG1 and NF in a transverse section of an intact nerve (A) and grayscale images of NDRG1 (B,D,F) and S-100 (C,E,G), in which each of the images is separately displayed, in longitudinal sections of an intact nerve (B,C) and the distal stumps of nerves at 2 days (D,E) and 9 days (F,G) after crush injury. **A–C:** In intact nerves the distribution of NDRG1 (gray in A) and NF immunoreactivity (white in A) is clearly distinguished, since the former is seen in the periphery (cf. Fig. 2A′) of the round profile of each fiber and the latter is in the center. On the other hand, the NDRG1-ir sites (B) are almost identical to the S-100-ir sites (C), suggesting that NDRG1 is localized in the cytoplasm of Schwann cells, but not in axons. **D–G:** At 2 days, the expression of NDRG1 (D) is maintained in the S-100-ir Schwann cells which have transformed into myelin-phagocytosing cells (E), but at 9 days, the expression (F) is hardly detected in S-100-ir Schwann cells with a irregular profile (G). Scale bar = 10 μm.

carcinoma BeWo (Xu et al., 1999). The expression of NDRG1 protein was upregulated in the macrophage differentiation of leukemic U937 cells induced by treatment with 1,25-$(OH)_2$ vitamin D_3 or retinoic acid (Piquemal et al., 1999). Furthermore, stable transfection of a colon cancer cell line with NDRG1 cDNA

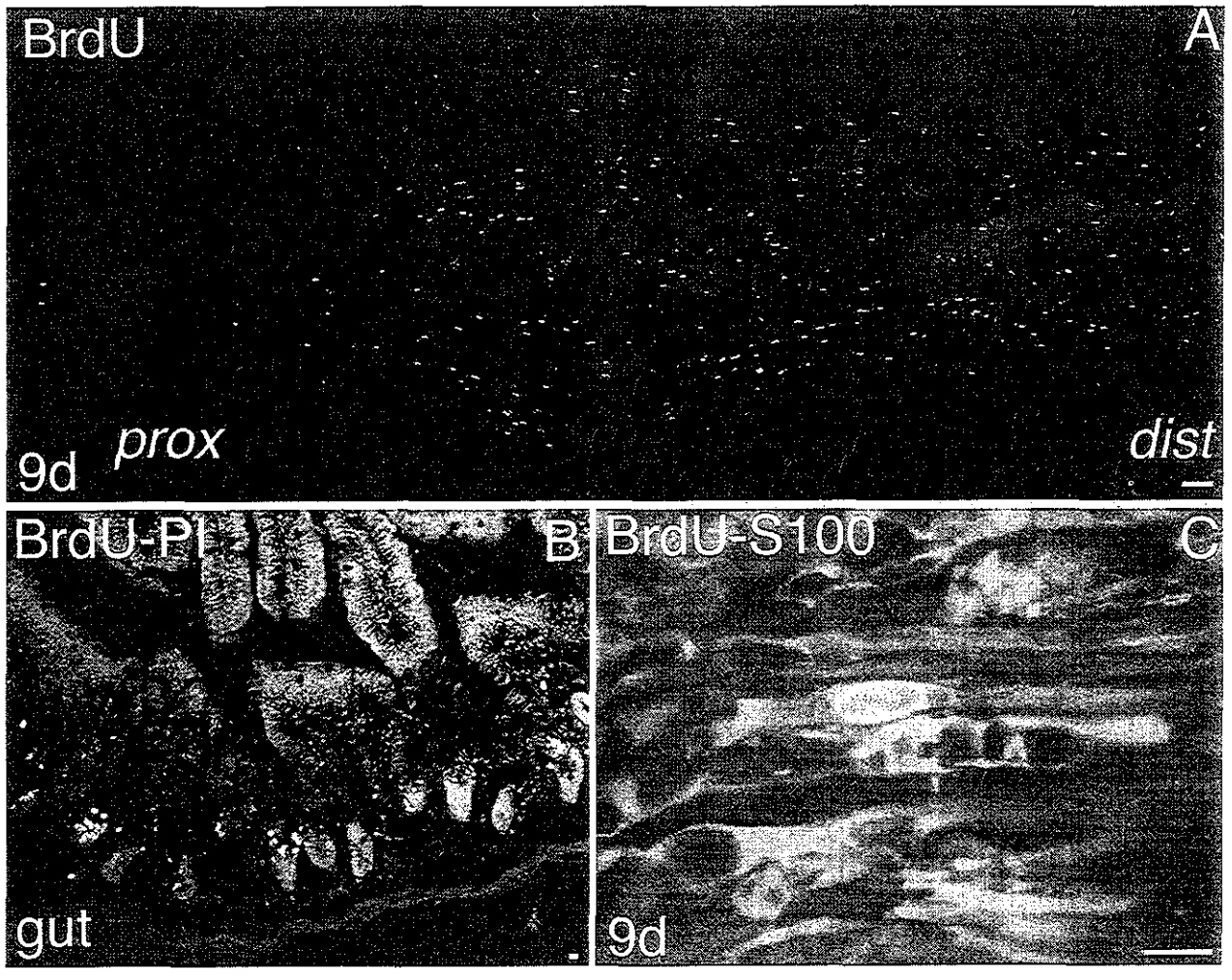

Fig. 4. BrdU immunofluorescent labeling of the nerve at 9 days after crush injury (**A,C**) and normal mouse jejunum as a positive control (**B**). **A:** In a longitudinal section of the nerve BrdU-labeled cells (white) are only distributed in the distal stump and the injury site, corresponding to the area where a marked depletion of NDRG1 is seen (cf. Fig. 1C). **B:** In a transverse section of the gut BrdU-labeled epithelial cells (white) are only located in the base of the crypts, to which cell proliferation is known to be restricted. Gray indicates PI-stained structures. **C:** In a higher-magnification image of the distal stump the double immunofluorescent labeling of BrdU (white) and S-100 (gray) shows that the nucleus of an S-100-ir cell is positive for BrdU, suggesting the mitotic activity of Schwann cells. Scale bars = 50 μm in A; 10 μm in B,C.

induced morphological and phenotypic changes indicative of differentiation, suggesting its possible role as a metastatic suppresser gene (Guan et al., 2000). Kurdistani et al. (1998) demonstrated that this gene was a p53-responsive gene with anti-proliferative properties, and that it was regulated in a cell cycle-dependent manner. These in vitro findings were supported by in vivo observations using in situ hybridization or immunohistochemical techniques showing that NDRG1 was expressed in the terminally differentiated cells in some organs, in which cell renewal is detectable under physiological conditions, such as colon epithelial cells (van Belzen et al., 1997), and skin keratinocytes (Gomez-Casero et al., 2001). Our immunohistochemical study on injured sciatic nerves revealed that the expression of NDRG1 was depleted in de-differentiated SCs and recovered in re-differentiated SCs with more immunoreactivity than that in the SCs of intact nerves. Thus, our findings suggest a role for NDRG1 in the terminal differentiation, including myelination, of SCs in nerve regeneration.

In a patient with HMSNL in whom a premature termination codon of the NDRG1 gene was found, one of the main neuropathological features of the disease was SC dysfunction, such as hypomyelination and demyelination/remyelination, failure of compaction of the innermost myelin lamellae, and poor hypertrophic response to the demyelination process (Kalaydjieva et al., 2000). It seems reasonable to surmise that this may be a direct effect of NDRG1 dysfunction, because this protein resides in SCs, especially myelinating ones. Kalaydjieva et al. (2000) inferred that the putative phosphopantetheine-binding domain present in NDRG1 protein (Kokame et al., 1996) may possibly be involved

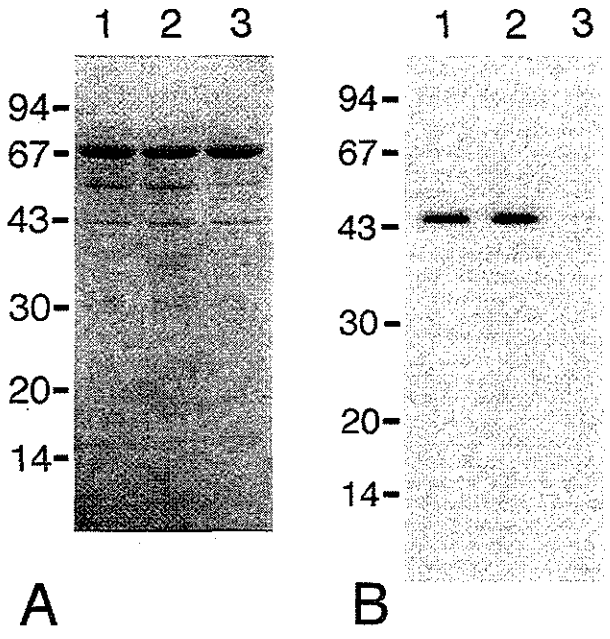

Fig. 5. Immunoblotting analysis of mouse sciatic nerves with a rabbit pAb to NDRG1. The samples were obtained at 9 days after crush injury. The amido black-stained sodium dodecyl sulfate-polyacrylamide gel electrophoresis (SDS-PAGE) profiles (**A**) and immunoblotted samples (**B**) from the intact side (**lane 1**), and the proximal stump (**lane 2**) and distal stump (**lane 3**) of the operated side are shown. The molecular weight markers (kDa) are indicated on the left.

in the lipid biosynthetic pathways operating in the myelinating SCs. On the other hand, Lachat et al. (2002) pointed out that the decompaction of the myelin sheath in the disease may be due to dysfunction of the adherens junctions in Schmidt-Lanterman incisures (Colman et al., 2001) based on their immunohistochemical findings that in all the examined epithelial cell types membrane labeling was observed predominantly adjacent to adherens junctions. Another prominent neuropathological feature of HMSNL is axonal involvement, such as early, severe, and progressive axonal loss (Kalaydjieva et al., 2000). Kalaydjieva et al. (2000) interpreted that NDRG1 may also have a role in the PNS, possibly in the SC signaling necessary for axonal survival, from their assumption that NDRG1 is possibly involved in SC differentiation, since differentiating SCs are an important source of signals for the development of nerves, in addition to controlling neuronal survival (Jessen and Mirsky, 1999). Our findings for NDRG1 expression in the process of nerve regeneration appear to support their hypothesis. However, further study is needed to clarify the exact role of NDRG1 in nerve development, since recent studies have stressed that the developmental process of the nerves is not always identical to the regenerative process, especially regarding the molecular mechanisms regulating SC proliferation (Kim et al., 2000; Atanasoski et al., 2001).

Besides the involvement of the NDRG1 in cell differentiation, this gene has been reported to be modulated under conditions of cellular stress that were caused by homocysteine (Kokame et al., 1996; Agarwala et al., 2000), forskolin (Xu et al., 1999), androgen (Segawa et al., 2002), nickel exposure (Salnikow et al., 2000), and hypoxia (Salnikow et al., 2000; Lachat et al., 2002). Our previous studies demonstrated that two different kinds of heat shock proteins (HSPs), 32 kDa-heat shock protein (Hirata et al., 2000) and 27 kDa-heat shock protein (Hirata et al., 2003) were differentially induced in different phases of SCs after axotomy, since the former was induced in SCs that transformed into myelin-phagocytosing cells immediately after the injury, while the latter was induced in SCs in the next phase that formed the SC column for axonal guidance. In the present study, NDRG1 was reexpressed during remyelination with more immunoreactivity than the normal level, suggesting its involvement in myelination, which is the last phase of SC transformation. No previous investigators have reported that the NDRG1 belongs to the HSPs. However, it is likely that, in addition to HSP32 and HSP27, this protein could be acting as a molecular base, explaining the inherent ability of SCs to not only protect themselves from abnormal environments but also participate actively in the repair process, although it may play a role in maintaining tissue homeostasis in intact nerves.

ACKNOWLEDGMENTS

The authors thank Mr. Yasuhiro Hirakawa and Mr. Takaaki Kanemaru (Morphology Core, Graduate School of Medical Sciences, Kyushu University) for their help in preparing the photomicrographs, and Mr. Naoya Inakura for his expert technical assistance.

REFERENCES

Agarwala KL, Kokame K, Kato H, Miyata T. 2000. Phosphorylation of RTP, an ER stress-responsive cytoplasmic protein. Biochem Biophys Res Commun 272:641–647.

Atanasoski S, Shumas S, Dickson C, Scherer SS, Suter U. 2001. Differential cyclin D1 requirements of proliferating Schwann cells during development and after injury. Mol Cell Neurosci 18:581–592.

Bandyopadhyay S, Pai SK, Gross SC, Hirota S, Hosobe S, Miura K, Saito K. Commes T, Hayashi S, Watabe M, Watabe K. 2003. The Drg-1 gene suppresses tumor metastasis in prostate cancer. Cancer Res 63:1731–1736.

Colman DR, Pedraza L, Yoshida M. 2001. Concepts in myelin sheath evolution. In: Jessen KR, Richerdson WD, editors. Glial cell development. 2nd ed. Oxford: Oxford University Press. p 161–176.

Fawcett JW, Keynes RJ. 1990. Peripheral nerve regeneration. Annu Rev Neurosci 13:43–60.

Gomez-Casero E, Navarro M, Rodriguez-Puebla ML, Larcher F, Paramio JM, Conti CJ, Jorcano JL. 2001. Regulation of the differentiation-related gene Drg-1 during mouse skin carcinogenesis. Mol Carcinogen 32:100–109.

Guan RJ, Ford HL, Fu Y, Li Y, Shaw LM. Pardee AB. 2000. Drg-1 as a differentiation-related, putative metastatic suppressor gene in human colon cancer. Cancer Res 60:749–755.

Hirata K, Kawabuchi M, 2002. Myelin phagocytosis by macrophages and nonmacrophages during Wallerian degeneration. Microsc Res Tech 57:541–547.

Hirata K, Mitoma H, Ueno N, He J, Kawabuchi M. 1999. Differential response of macrophage subpopulations to myelin degradation in the injured rat sciatic nerve. J Neurocytol 28:685–695.

Hirata K, He J, Kuraoka A, Omata Y, Hirata M, Shariful Islam ATM, Noguchi M, Kawabuchi M. 2000. Heme oxygenase 1 (HSP-32) is induced in myelin-phagocytosing Schwann cells of injured sciatic nerves in the rat. Eur J Neurosci 12:4147–4152.

Hirata K, He J, Hirakawa Y, Liu W, Wang S, Kawabuchi M. 2003. HSP27 is markedly induced in Schwann cell columns and the associated regenerating axons. Glia 42:1–11.

Jessen KR, Mirsky R. 1999. Schwann cells and their precursors emerge as major regulators of nerve development. Trends Neurosci 22:402–410.

Kalaydjieva L, Gresham D, Gooding R, Heather L, Baas F, de Jonge R, Blechschmidt K, Angelicheva D, Chandler D, Worsley P, Rosenthal A, King RH, Thomas PK. 2000. N-myc downstream-regulated gene 1 is mutated in hereditary motor and sensory neuropathy-Lom. Am J Hum Genet 67:47–58.

Kim HA, Pomeroy SL, Whoriskey W, Pawlitzky I, Benowitz LI, Sicinski P, Stiles CD, Roberts TM. 2000. A developmentally regulated switch directs regenerative growth of Schwann cells through cyclin D1. Neuron 26:405–416.

Kokame K, Kato H, Miyata T. 1996. Homocysteine-respondent genes in vascular endothelial cells identified by differential display analysis. GRP78/BiP and novel genes. J Biol Chem 271:29659–29665.

Krauter-Canham R, Bronner R, Evrard JL, Hahne G, Friedt W, Steinmetz A. 1997. A transmitting tissue- and pollen-expressed protein from sunflower with sequence similarity to the human RTP protein. Plant Sci 129:191–202.

Kurdistani SK, Arizti P, Reimer CL, Sugrue MM, Aaronson SA, Lee SW. 1998. Inhibition of tumor cell growth by RTP/rit42 and its responsiveness to p53 and DNA damage. Cancer Res 58:4439–4444.

Lachat P, Shaw P, Gebhard S, van Belzen N, Chaubert P, Bosman FT. 2002. Expression of NDRG1, a differentiation-related gene, in human tissues. Histochem Cell Biol 118:399–408.

Lin TM, Chang C. 1997. Cloning and characterization of TDD5, an androgen target gene that is differentially repressed by testosterone and dihydrotestosterone. Proc Natl Acad Sci USA 94:4988–4993.

Melhem MF, Meisler AI, Finley GG, Bryce WH, Jones MO, Tribby II, Pipas JM, Koski RA. 1992. Distribution of cells expressing myc proteins in human colorectal epithelium, polyps, and malignant tumors. Cancer Res 52:5853–64.

Nishie A, Masuda K, Otsubo M, Migita T, Tsuneyoshi M, Kohno K, Shuin T, Naito S, Ono M, Kuwano M. 2001. High expression of the Cap43 gene in infiltrating macrophages of human renal cell carcinomas. Clin Cancer Res 7:2145–2151.

O'Daly JA, Imaeda T. 1967. Electron microscopic study of Wallerian degeneration in cutaneous nerve caused by mechanical injury. Lab Invest 17:744–766.

Okuda T, Kondoh H. 1999. Identification of new genes ndr2 and ndr3 which are related to Ndr1/RTP/Drg1 but show distinct tissue specificity and response to N-myc. Biochem Biophys Res Commun 266: 208–215.

Piquemal D, Joulia D, Balaguer P, Basset A, Marti J, Commes T. 1999. Differential expression of the RTP/Drg1/Ndr1 gene product in proliferating and growth arrested cells. Biochim Biophys Acta 1450: 364–373.

Potten CS, Booth C, Pritchard DM. 1997. The intestinal epithelial stem cell: the mucosal governor. Int J Exp Pathol 78:219–243.

Qu X, Zhai Y, Wei H, Zhang C, Xing G, Yu Y, He F. 2002. Characterization and expression of three novel differentiation-related genes belong to the human NDRG gene family. Mol Cell Biochem 229:35–44.

Salnikow K, Blagosklonny MV, Ryan H, Johnson R, Costa M. 2000. Carcinogenic nickel induces genes involved with hypoxic stress. Cancer Res 60:38–41.

Sato N, Kokame K, Shimokado K, Kato H, Miyata T. 1998. Changes of gene expression by lysophosphatidylcholine in vascular endothelial cells: 12 up-regulated distinct genes including 5 cell growth-related, 3 thrombosis-related, and 4 others. J Biochem 123:1119–26.

Segawa T, Nau ME, Xu LL, Chilukuri RN, Makarem M, Zhang W, Petrovics G, Sesterhenn IA , McLeod DG, Moul JW, Vahey M, Srivastava S. 2002. Androgen-induced expression of endoplasmic reticulum (ER) stress response genes in prostate cancer cells. Oncogene 21:8749–8758.

Shaw E, McCue LA, Lawrence CE, Dordick JS. 2002. Identification of a novel class in the alpha/beta hydrolase fold superfamily: the N-myc differentiation-related proteins. Proteins 47:163–168.

Shimono A, Okuda T, Kondoh H. 1999. N-myc-dependent repression of ndr1, a gene identified by direct subtraction of whole mouse embryo cDNAs between wild type and N-myc mutant. Mech Dev 83:39–52.

Stoll G, Griffin JW, Li CY, Trapp BD. 1989. Wallerian degeneration in the peripheral nervous system: participation of both Schwann cells and macrophages in myelin degradation. J Neurocytol 18:671–683.

Ulrix W, Swinnen JV, Heyns W, Verhoeven G. 1999. The differentiation-related gene 1, Drg1, is markedly upregulated by androgens in LNCaP prostatic adenocarcinoma cells. FEBS Lett 455:23–26.

van Belzen N, Dinjens WN, Diesveld MP, Groen NA, van der Made AC, Nozawa Y, Vlietstra R, Trapman J, Bosman FT. 1997. A novel gene which is up-regulated during colon epithelial cell differentiation and down-regulated in colorectal neoplasms. Lab Invest 77:85–92.

Xu B, Lin L, Rote NS. 1999. Identification of a stress-induced protein during human trophoblast differentiation by differential display analysis. Biol Reprod 61:681–686.

Yamanaka I, Kuraoka A, Inai T, Ishibashi T, Shibata Y. 1997. Changes in the phosphorylation states of connexin43 in myoepithelial cells of lactating rat mammary glands. Eur J Cell Biol 72:166–173

Zhou D, Salnikow K, Costa M. 1998. Cap43, a novel gene specifically induced by Ni2+ compounds. Cancer Res 58:2182–2189.

Journal of the Peripheral Nervous System 9:144–157 (2004)

RESEARCH REPORT

The spatiotemporal characterization of endplate reoccupation, with special reference to the superposition patterns of the presynaptic elements and the postsynaptic receptor regions during muscle reinnervation

Songyan Wang, Masaru Kawabuchi, Chong Jian Zhou, Kazuho Hirata, Huibing Tan, and Akio Kuraoka

Department of Anatomy and Cell Biology, Graduate School of Medical Sciences, Kyushu University, Fukuoka, Japan

Abstract In this study, an immunohistochemical investigation was carried out to define spatiotemporal characteristics of superposition patterns of the presynaptic elements and the postsynaptic acetylcholine receptor (AChR) sites during the period of endplate regeneration after sciatic nerve crush. The extent of close correspondence of terminal Schwann cell (TSC)-, or axon terminal-, apposing AChR sites was quantitated with three-dimensional images of neuromuscular junctions (NMJs) taken under confocal laser-scanning microscopy. After 3-weeks post-crush (wpc), reoccupation of regenerating TSCs and later arriving axon terminals proceeded within the scope of previously denervated AChR plaques. During this period, the areas of presynaptic elements and the areas of postsynaptic elements were highly correlated. TSCs rapidly reoccupied a greater part of the postsynaptic receptors. In contrast, there was a slower increase of the contact areas of AChR sites overlapped by the axon terminals. Reoccupation by the presynaptic elements at 20 wpc was almost completed in a majority of NMJs, but some anomalous changes still continued to occur in a small proportion of the NMJs (20–30%). Our results suggest that: (a) with gradual increase of the contact areas between presynaptic and postsynaptic elements, imperfect reinnervation and regeneration, due to spatial mismatching or unbalanced growth between presynaptic and postsynaptic elements, result in sporadic remodeling; (b) the difference in superposition patterns between TSCs and axon terminals depends on the ability of making alignment to the endplate gutters in regenerating NMJs; and (c) a complex set of anatomical relationships among the three endplate components affects the process of endplate reoccupation synthetically.

Key words: acetylcholine receptor, immunohistochemistry, nerve regeneration, neuromuscular junction, Schwann cell

Introduction

In our recent study, the reinnervation of individual muscle fibers was investigated at various time points after the sciatic nerve was crushed *(Kawabuchi et al., 1998; 2001)*. After 3-weeks post-crush (wpc), the reinnervating Schwann cells (SCs) reoccupied damaged endplates by growing through the original SC tubes. At the later time, returned axons began to reoccupy damaged endplates, and over the following weeks, most endplates become gradually recovered. Terminal differentiation and endplate reoccupation were in process during the first few months of the reinnervation

Address correspondence to: Masaru Kawabuchi, MD, PhD, Department of Anatomy and Cell Biology, Graduate School of Medical Sciences, Kyushu University, Higashi Ku, Maidashi 3-1-1, Fukuoka 812-8582, Japan. Tel: +81-92-642-6045; Fax: +81-92-642-6050; E-mail: kawabuchi@helen.ocn.ne.jp

period, with a concomitant regenerative growth of the terminal SCs (TSCs) and the sites of clustered acetylcholine receptors (AChRs) *(Kawabuchi et al., 2001)*.

Normally, there is a precise spatial alignment between the presynaptic and postsynaptic elements in the vertebrate neuromuscular junctions (NMJs), which alters during remodeling, development, and regeneration. From the *in vivo* visualization study of the mammalian NMJs in living animals, the location of axon terminals, TSCs, and the distribution of AChR in the postsynaptic muscle fiber membrane were investigated during the period of muscle reinnervation *(Rich and Lichtman, 1989; O'Malley et al., 1999)* or muscle fiber growth *(Balice-Gordon and Lichtman, 1993)*. In both regeneration and growth, loss of AChR from a portion of the synapse precedes a rapid, partial loss of nerve terminal branches. In regeneration, the axon terminal precisely reoccupies the receptor regions in the old endplate site of the adult muscle *(Rich and Lichtman, 1989)*.

The three cellular components of NMJs, TSCs, motor axon terminals, and postsynaptic muscle fibers, are known to perform interaction that affects synapse formation, maintenance, and repair *(Hall and Sanes, 1993; Burden, 1998)*. The synaptic basal lamina contains a number of signaling proteins that influence motor nerve terminal differentiation during muscle reinnervation *(Sanes et al., 1978; Glicksman and Sanes, 1983; Sanes, 2003)*. The TSCs may regulate some aspects of differentiation and maintenance of axon terminals *(Jahromi et al., 1992; Rochon et al., 2001)* and synaptic plasticity *(Robbins and Polak, 1988)*. In addition, TSCs play a role in muscle reinnervation, and processes extended by TSCs after denervation influence the regrowth of motor axons to the muscles and their guidance back to denervated NMJs *(Son and Thompson, 1995a; 1995b; Trachtenberg and Thompson, 1997; O'Malley et al., 1999)*. At the same time, motor axon terminals also play a role in postsynaptic differentiation. Finally, it is generally agreed that besides providing the trophic support for neurons *(Grinnell and Herrera, 1981; Wernig and Herrera, 1986)*, feedback mechanisms from the muscle are important to anatomically or physiologically align neuromuscular synapses to their target cells *(Nudell and Grinnel, 1983; Slack et al., 1983; Hopkins et al., 1985; Crews and Wigston, 1990; Kuno, 1990)*.

Confocal three-dimensional (3D) images are useful for visualization and the morphological analysis of structures in regenerating NMJs. The advantage of this technique, compared with that performed by conventional fluorescence microscopy, is introduced below. Compared to normal junctions, regenerating neural elements are initially smaller and show various structural changes, such as uneven outlines and wide variability in size and terminal morphology. For those structures that originally have curvature and change with time, the 3D structure is more powerful in representing the true planar area of the endplate.

Knowledge of how TSCs or axons respond to nerve injury, particularly when reoccupation takes place on the once denervated postsynaptic receptor region, is important for understanding the formation and maintenance of regenerating NMJs. Following regeneration after nerve crush, the superimposed images of the TSC or axon terminal and AChR sites within the endplate of rat muscle were measured utilizing a dual-color confocal imaging technique *(Kawabuchi et al., 2001)*. In this study, we extend our previous observations by demonstrating some particular features of superposition of the presynaptic elements in relation to the postsynaptic elements in the spatiotemporal course of endplate reoccupation. In addition, the close correspondence (CC) between the pre- (TSC- or axon terminal-occupied region) and postsynaptic region was investigated quantitatively to define the difference in superposition patterns between the TSCs and axon terminals. Motor endplates were visualized by labeling the AChR sites with fluorescein isothiocyanate (FITC)-conjugated α-bungarotoxin (α-BT). Cryosections of the rat skeletal muscle were double-labeled with SC marker (S100) and α-BT, or with axonal marker (PGP9.5) and α-BT, and then observed using confocal laser-scanning microscopy. PGP9.5 is a suitable marker for detection of regenerating axons reinnervating in different target organs and is helpful for locating the major nerve pathways through target tissue (e.g., skin and muscle) *(Hirata et al., 1997; Navarro et al., 1997; Verdú and Navarro, 1997; Kawabuchi et al., 2001)*.

Despite return of motor nerve processes within weeks to months after peripheral nerve lesions, recovery of motor function is delayed for years *(Bowe et al., 1989)*. To evaluate the magnitude of restoration of the original motor function following peripheral nerve injury, long-term observations on the process of incomplete regeneration and reinnervation in NMJs need to be presented. In the present study, long-term alterations in the spatiotemporal course of endplate reoccupation, which persisted after regenerating axons grow into NMJs, were examined for up to 20 weeks.

Materials and Methods

Animals

All procedures were approved by the Committee of Ethics on Animal Experiments in the Faculty of Medicine, Kyushu University. Fifty adult male rats

(4 months old; body weight 315 ± 19 g, Wistar/Ms) were used for the experiments.

Surgery and tissue preparation

The procedures for nerve crush were the same as previously reported *(Kawabuchi et al., 1998)*. Under deep ether anesthesia followed by pentobarbital sodium (50 mg/kg body weight, subcutaneous injection), the right sciatic nerve was exposed and crushed for 20 s with microforceps. After nerve crush was achieved at the maximum pressure, the wound was sutured and animals were allowed to recover. At the time of perfusion, the operated leg muscles were found to become smaller than those of the control side in all cases in this study. A 15–25% reduction in muscle weights at 4 wpc was noted.

The animals were divided into several groups and allowed to survive for 1, 3, 4, 6, 8, 12, and 20 weeks post nerve crush. The soleus muscles from four to six rats were examined in each group; the muscles from control side served as control. In addition, 12 animals were divided equally into four groups, which were allowed to survive without operation for 4, 8, 12, and 20 weeks, to serve as negative controls. Three adult rats were used as sham operated ($n = 3$) controls, where the nerve was exposed but not damaged. Following ether anesthesia and pentobarbital sodium, the animals were perfused through the aorta with phosphate-buffered saline (PBS) (pH 7.6) followed by 300–500 mL of fixative composed of 4% paraformaldehyde in 0.1 M phosphate buffer at pH 7.4. The muscles were dissected out and were then immersed in graded sucrose solution (up to 20% in 0.1 M phosphate buffer) for cryo-protection. A series of 50-μm-thick longitudinal serial sections were cut on a cryostat microtome (Frigocut, Germany) at −20 °C and were collected in PBS.

Immunohistochemistry

Sections were rinsed twice in PBS and once in 0.4% Triton-X 100 in PBS for 10 min, respectively, and then incubated in 1% bovine serum albumin (BSA) in PBS supplemented with 0.05% NaN_3 for 1 h. The following primary antibodies were applied to the sections for 24–48 h at room temperature: polyclonal anti-PGP9.5 (Ultraclone) diluted at 1 : 1,600–2,000 and polyclonal anti-S100 (Nichirei) diluted at 1 : 40. For detection of bound antibodies, the following procedures were used: sections were incubated with biotinylated secondary antisera (goat anti-rabbit IgG) diluted at 1 : 200 (Vector Laboratories, Burlingame, CA, USA) for 3 h, followed by streptavidin labeled with Texas red diluted at 1 : 200 (Vector Laboratories) for 2 h. Between each step, sections were washed three times in PBS for 15–30 min. All procedures were performed at room temperature (about 20 °C). The sections were placed on a slide pretreated with 0.1% Poly-L-Lysine (Sigma). Following immunostaining, the area of the postsynaptic AChR site was defined by FITC-conjugated α-BT staining for 1 h at 37 °C (dilution 1 : 200, Molecular Probes, Eugene, OR). Then sections were washed several times in PBS for 30 min and mounted with Vectashield (Vector, USA).

Confocal laser-scanning microscopy

Counterstained materials were observed with a confocal laser-scanning microscopy system (CLSM-GB 200 Olympus, Japan) equipped with an argon/krypton ion laser, allowing simultaneous scanning of two fluorescent dyes. In order to avoid any nonspecific cross-talk, observations of staining for either FITC or Texas red were made as the following: the wave length of the excitation laser light was restricted to 488 nm (argon laser) for FITC or to 568 nm (krypton laser) for Texas red separately by switching the dichroic mirrors. For simultaneous observations of the materials double-stained by FITC and Texas red, the serial images were taken under 488 nm and 568 nm laser lights separately on the same scope. Optical sections at intervals of 0.5–1 μm were projected on a single plane extending in 10–40 μm thickness. The series of optical sections were reconstructed to show superimposed images of the TSC and AChR site or axon terminal and AChR site. Using a 40× or 60× water immersion objective lens, the 3D structure of the motor endplate can be shown by reconstructing the series of images. It was noted that the areas of endplates on the adult muscle in 3D image are significantly larger than that in 2D image.

Morphometric analysis

For quantitative analysis of each of the three-dimensionally reconstructed junctional components, several sections in 50 μm thickness with the necessary number of NMJs were selected from each animal. To combine the data from different animals, all the sections from three to six animals in each group were processed for morphometry. In addition, it was determined that at least 15 NMJs per section and five sections per animal were required for statistical reliability to ensure that inter-animal variability was not significant. Only the motor endplates cut at the tangential plane were selected and images in which the entire motor endplate was parallel to the long axis of the muscle fiber were rejected. The area of motor endplate was defined as where the preterminal SCs or axons terminate on the AChR sites outlined by α-BT staining. One motor endplate was often organized into two or more groups, each of which contained a collection of terminal SCs or nerve terminal branches. To

avoid errors in statistical reliability, the motor endplates with undefined borders, due to distant neighboring groups of TSCs or axon terminals, were not counted. The area of an axon terminal included the projection area of the axon terminal and its branches at the AChR site, and the point of origin was defined as the first branch point of the axon terminal.

The time course of changes in sizes of S100-like immunoreactive TSCs, PGP9.5-like immunoreactive axon terminals, and α-BT-stained AChR sites was documented in our previous study *(Kawabuchi et al., 2001)*. In the present study, individual sizes during regenerative growth at 4, 8, 12, and 20 wpc, estimated from the extent of the longitudinal-sectional areas, were combined in a scatter diagram, and the distribution of individual value pairs for the area of presynaptic elements (TSCs or axon terminals) and AChR sites is shown (Fig. 1). The anatomical relationship between these parameters was analyzed by single-variance linear regression analysis. Single Texas red-stained S100- or PGP9.5-like immunoreactivity was normally red, but it would become yellow when structures

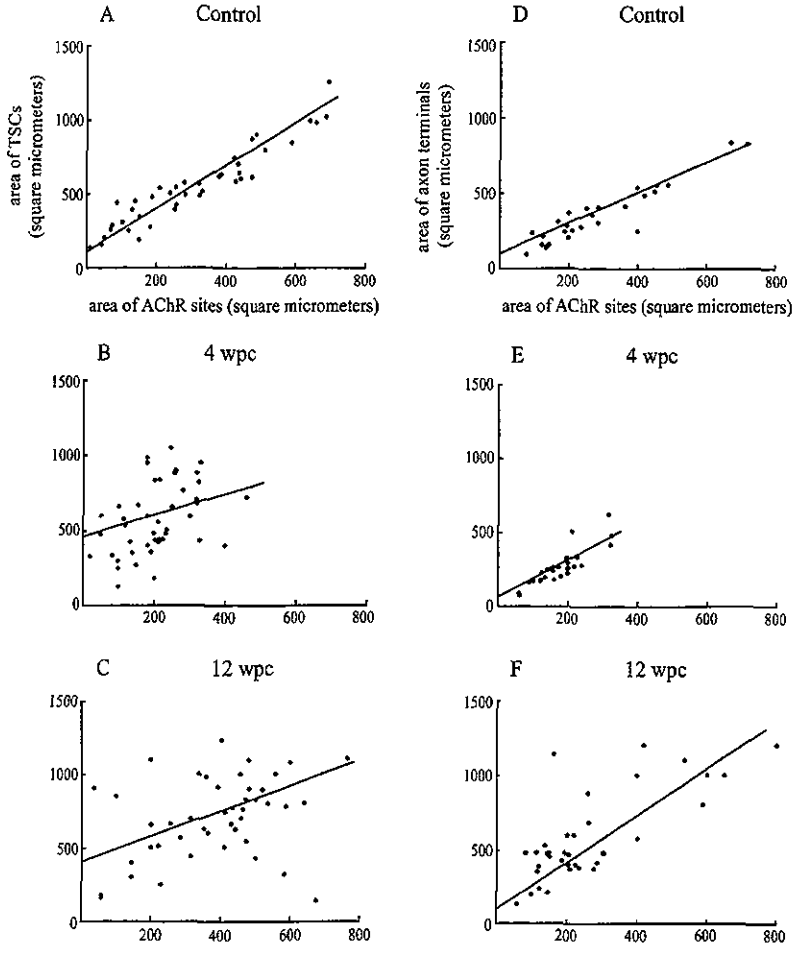

Figure1. Scatter diagrams of the relationship between area (μm^2) of acetylcholine receptor (AchR) sites (horizontal axis) and area of terminal Schwann cell (TSCs) (A–C) or area of axon terminals (D–F) in neuromuscular junctions (NMJs) (vertical axis). Measurements were performed on 90–150 samples from control (A and D), 4-weeks post-crush (wpc) (B and E) and 12 wpc (C and F) separately. The unit values are indicated by a square. The regression line is calculated from the pooled values of the two data sets. (A) The increase in area of the AChR sites in control correlates with that of the TSCs [r (correlation efficient) = 0.94, $p < 0.001$, two-tailed t-test, $n = 97$]. (B, C) The shift of individual value pairs at 4 and 12 wpc indicates that nerve crush induced a decrease in areas of AChR-rich sites and correlated changes in areas of TSCs ($r = 0.42$ at 4 wpc, $p < 0.001$, two-tailed t-test, $n = 62$; $r = 0.33$ at 12 wpc, $p < 0.01$, $n = 145$). The distribution of points at 12 wpc seems to be more dispersed than at 4 wpc. (D) A significant linear relationship is obtained between the two parameters in the control [r (correlation efficient) = 0.93, $p < 0.001$, two-tailed t-test, $n = 97$]. (E, F) At 4 and 12 wpc, there is the similar linear relationship between area of axon terminals and area of AChR sites in NMJs ($r = 0.86$ at 4 wpc, $p < 0.001$, two-tailed t-test, $n = 62$; $r = 0.75$ at 12 wpc, $p < 0.01$, $n = 145$). The shift of individual value pairs at 4 wpc indicates that nerve crush induced a coincidental decrease between TSCs and AChR plaques. (F) Note considerable correlated recovery in the 12-week muscles.

were identified by both Texas red staining and green FITC fluorescence, where superimposition of presynaptic elements and postsynaptic receptor regions existed. A schematic representation of the analysis for superimposed images from the region of CC, estimated by the programs Adobe Photoshop and NIH, is shown in Fig. 2. In order to make an easy morphometric analysis, the double-color images (see boxed regions in Fig. 3C,I) were converted to single-color image at first, by switching the multiple color channels to only one channel with Photoshop (green for FITC or red for Texas red). Then the single-color images were converted to gray (black and white) images by grayscale mode, which can show the areas of TSCs, axon terminals, or AChR sites separately (Fig. 2). In addition, for analysis of the superimposed yellow areas between TSC/AChR site or axon terminal/AChR site in double-color images (see boxed areas in Fig. 3), the double-color images were converted to gray images with Photoshop (Fig. 2). Then the gray images were processed by threshold mode, and the threshold intensity on the grayscale image was adjusted by density-slice filtering. With appropriate adjustment, the non-overlapped areas from presynaptic and postsynaptic elements were then taken away from the NMJ by digitally subtracting the binary image and the accurate superimposed areas were displayed (Fig. 2). Selected superimposed areas corresponding to the CC were

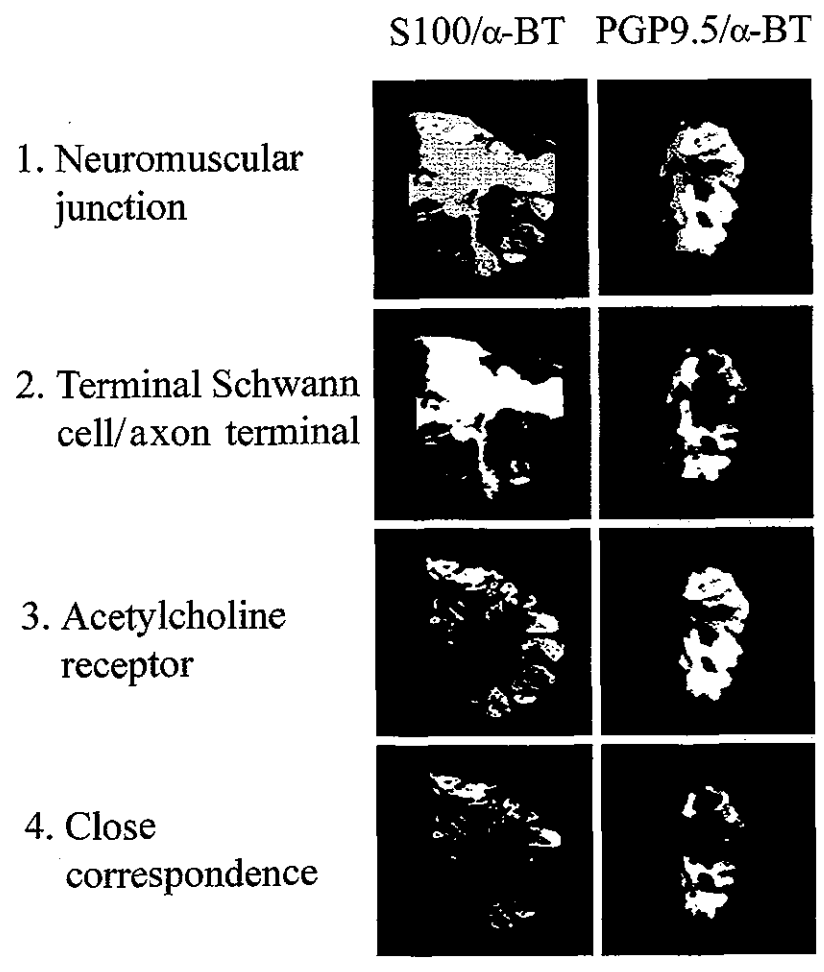

Figure 2. Diagrammatic procedure for estimating extent of close correspondence (CC) between pre- and postsynaptic elements of neuromuscular junctions (NMJs). The dual-color images of the original double-labeled fluorescent NMJs are from the boxed regions in Fig. 3(C,I). Terminal Schwann cells (TSCs) or axon terminals are shown in red, receptor regions in green, and the superimposed regions [CC with the postsynaptic acetylcholine receptor (AchR) sites] in yellow. (1) The original color images are converted to Gray images. (2), (3), and (4) grayscale images are converted to binary images, using an intensity threshold based on the mean background level. (2) The binary image of the TSC or axon terminal is digitally subtracted from the binary image of the NMJ. (3) The receptor regions demonstrate branches associated with disparate clusters of AChRs. (4) The area of CC is obtained by digitally subtracting the area of non-correspondence from the total area of the receptor region. In addition, the binary subtraction images in (4) are independently verified by referring to the original yellow-colored images in boxed areas of Fig. 3(C,I).